Journal of Molecular Graphics and Modelling 40 (2013) 91–98

Contents lists available at SciVerse ScienceDirect

Journal of Molecular Graphics and Modelling

journal homepage: www.elsevier.com/locate/JMGM

Assessment of new anti-HER2 ligands using combined docking, QM/MM scoring and MD simulation

Marawan Ahmed[a,*], Maiada M. Sadek[b], Rabah A. Serrya[c], Abdel-Hamid N. Kafafy[d], Khaled A. Abouzid[c], Feng Wang[a]

[a] eChemistry Laboratory, Faculty of Life and Social Sciences, Swinburne University of Technology, Melbourne, Victoria 3122, Australia
[b] Pharmaceutical Organic Chemistry, Faculty of Pharmacy, MSA University, 6th October, Egypt
[c] Pharmaceutical Chemistry Department, Faculty of Pharmacy, Ain Shams University, Cairo 11566, Egypt
[d] Pharmaceutical Organic Chemistry Department, Faculty of Pharmacy, Assiut University, Egypt

ARTICLE INFO

Article history:
Accepted 6 December 2012
Available online 17 December 2012

Keywords:
Protein kinase
HER2
Molecular dynamics
AMBER
QM/MM scoring

ABSTRACT

In the development of new anti-cancer drugs to tackle the problem of resistance to current chemotherapeutic agents, a new series of anti-HER2 (human epidermal growth factor receptors 2) agents has been synthesized and investigated using different computational methods. Although non-selective, the most active inhibitor in the new series shows higher activity toward HER2 than EGFR. The induced fit docking protocol (IFD) is performed to find possible binding poses of the new inhibitors in the active site of the HER2 receptor. Molecular dynamic simulations of the inhibitor–protein complexes for the two most active compounds from the new series are carried out. Simulations stability is checked using different stability parameters. Different scoring functions are employed.

1. Introduction

One of the major limitations of docking in computational drug design is the rigid receptor approach [1]. In general, the scoring function of any docking engine is designed to be fast and robust. However, to achieve this goal, important details of the binding process are approximated or even completely ignored. This can be justified especially when one is dealing with virtual libraries of thousands or even millions of compounds to be in silico screened. The rigid receptor approach can be safely pursued in closely related structures where it can perform appropriately, but for cases where ligand sets are diverse or where the protein is flexible, methods that can partially or fully account for protein flexibility may be more suitable. One of such methods involves an atomic vdW radii scaling, allowing ligand atoms to come close to receptor atoms without heavy penalties, i.e. "the soften-potential" method [2]. Another method allows certain amino acids residues to change conformation during the docking process [3].

The third method which is a "partially flexible" method is the induced fit docking (IFD) method [4]. In this method, both the ligand and amino acid residues side chains within a given radius around the binding pocket are allowed to move freely during the binding process, so that the side chains undergo "re-structuration" [5]. The "fully flexible" method, which accounts for the coupling between protein and ligand in the binding process is the molecular dynamic (MD) simulation, this method is still far from being used as a replacement for conventional docking. Molecular dynamics simulation is a valuable and routine tool in the process of drug discovery. It offers wide range of solutions for different problems that are encountered during the entire process of computational drug design. It can be used to refine protein–ligand complexes, calculating the binding energies, and several more [6].

Previous studies have shown that the IFD protocol is successful in various types of receptors, such as the highly flexible kinases [7,8]. In these studies, the IFD reproduces the experimentally measured binding pose of the ligand to various degrees of accuracy. In this regard, Zhong et al. [7] showed that IFD was able to reproduce the binding pose of a number of experimentally resolved crystal structures of different kinases complexed with their inhibitors to high accuracy. It was clearly demonstrated that the performance of the IFD method is superior to that of the Glide rigid receptor docking. For example, the IFD was able to reproduce the experimentally measured crystal structure of imatinib complexed with the inactive conformation of the ABL mutant (PDB code: 2GQG). The IFD protocol performed very well compared to the Glide rigid receptor approach [7].

Cancer is characterized by a high rate of mutation, which in many cases causes the current known inhibitors to be ineffective [9,10]. Kinases are known to be a viable target for anti-cancer drug development. A major type of kinases is the human epidermal

* Corresponding author. Tel.: +61 3 9214 8785.
E-mail address: mmahmed@swin.edu.au (M. Ahmed).

1093-3263/$ – see front matter © 2012 Elsevier Inc. All rights reserved.
http://dx.doi.org/10.1016/j.jmgm.2012.12.001

growth factor receptor tyrosine kinase 2 (HER2), for which several types of known inhibitors with various degrees of selectivity have been synthesized [11]. In the present study, the binding mode of a recently synthesized quinazoline based anti-HER2 (described elsewhere for their synthesis and biological evaluation) agents [12] is investigated using a combined method of IFD and molecular dynamic simulations, in order to reveal their inhibitory activity against HER2.

2. Methods and computational details

2.1. Protein and inhibitors preparation

Fig. 1 gives the crystal structure of the kinase domain of human epidermal growth factor receptor 2 (HER2, Fig. 1a) co-crystallized with the inhibitor (SYR127063, Fig. 1b), a pyrrolopyrimidine inhibitor (PDB entry: 3PP0) [13]. The co-crystallized binding mode of the inhibitor in the active site is also shown in the same figure (Fig. 1c). Docking calculations are carried out using the induced fit docking protocol (IFD workflow) in the Schrödinger suite [4,14]. The receptor is prepared using the protein preparation wizard in Maestro 9.2 [15]. The structure is in a dimer form, only one chain is kept. The structure is then saturated by hydrogen atoms, all free water molecules within 5 Å of the inhibitor are deleted but for a conserved water molecule (HOH), which is observed in the crystal structures of several kinases [16–19]. This bridge water molecule connects the N(3) of the quinazoline ring of the inhibitor to the side chain of Thr798, as shown in Fig. 1c. Missing residues are added and refined using Prime 3.0 [20,21]. An ACE (acetyl) and NMA (N-methyl amide) groups are added to cap the uncapped N and C termini.

Interactive hydrogen bond (H-bond) network optimization is carried out assuming a neutral pH. The protonation states of titratable amino acids are assigned at the same pH. Water orientation is positioned as shown in Fig. 1c, all atoms impref minimization step is carried out to convergence at a maximum RMSD of 0.3 Å from the original conformation. No steric clashes are reported after the final minimization step.

Fig. 2 gives the 2D structures of studied inhibitors, which are further optimized at the PM6 semiempirical level of theory using the Gaussian 09 computational chemistry program [22].

2.2. Induced fit docking

The IFD module in Schrödinger involves 3 main steps: docking, refinement and final re-docking [4,23,14]. All inhibitors are docked to the HER2 receptor (Fig. 1) using a softened-core potential by scaling the receptor atomic vdW radii by 0.7, and inhibitor atomic vdW radii by 0.5. The top 20 poses obtained are then subjected to Prime [20,21] side chain refinement for residues within 5 Å from any inhibitor pose. These new protein conformational structures are used for a conventional glide docking run with the default parameters. The initial phase of docking is run using the standard module of docking (Glide SP), the extra precision mode is used for the final stage of docking (Glide XP) [24,25]. An H-bond constraint in which the backbone amide group of Met801 serves as an H-donor to the N1 atom of the inhibitors is applied for both glide docking runs. Side chains of five residues are trimmed during the docking process. That is, Lys753, Glu770, Met774, Leu796 and Phe864.

2.3. Molecular dynamic setup

Two inhibitor–protein complexes (M8 and M19) obtained from the previous IFD runs are further subjected to extensive molecular dynamic simulations. The structure preparation and the following MD simulations are performed using AMBER 12 software package [26] applying the ff03 force field [27,28]. Single point calculations of the corresponding inhibitors are performed at the B3LYP/cc-pVTZ level of theory in ether ($\varepsilon = 4.2$) solvent applying the IEF-PCM model [29] using the Gaussian 09 program [22]. The inhibitor charges and other parameters are obtained using the RESP fitting [30] procedures and the general AMBER force field (GAFF) [31]. The complexes are then solvated with a box of TIP3P [32] water with a buffer size of 15 Å and are neutralized by counter ions.

Each system is then subjected to four consecutive minimization steps, in each step, water molecules and ions are allowed to move freely for a 1000 steps of steepest descent minimization followed by 4000 steps of conjugate gradient minimization holding protein and inhibitor atoms constrained to their original positions by a force constant of 100 kcal/mol/Å^2, then gradually releasing the force constraints to 50, 5 and 0 (no constraints) kcal/mol/Å, respectively. Following minimization, two consecutive steps of heating and equilibration are performed. The system is gradually heated in the NVT ensemble from 0°K to 300°K for 30 ps with a time step of 1 fs, applying a force constant of 10 kcal/mol/Å on the protein and inhibitor coordinates, and using Langevin dynamics with the collision frequency γ of 1 ps^{-1} for temperature control. A further 1 ns simulation in the NPT ensemble is performed to equilibrate the system density applying a time step of 2 fs, which requires the use of SHAKE algorithm [33] to constrain all bonds involving hydrogen atoms. The temperature is controlled using Langevin dynamics with the collision frequency γ of 1 ps^{-1} and is kept at 300°K. The pressure is kept at 1 bar applying a Berendsen barostate with a pressure relaxation time of 1 ps. Each system is again relaxed in the NVT ensemble for 1 ns followed by 10 ns production simulation in the NVT ensemble at 300°K using Berendsen temperature control [34]. In all simulation steps, long-range electrostatics are computed using the particle mesh Ewald (PME) [35] with a non-bonded cut off of 12 Å. The edge effect is removed by applying periodic boundary conditions. Binding energies are calculated from the MD trajectories using the PBSA module in AMBER12. All MD simulations are carried out using the PMEMD module of AMBER12.

2.4. MMPB/GBSA binding energy calculations

The binding energy calculations of the produced complexes are estimated using different methods based on the structures obtained from the IFD and MD simulations. The Prime-MM/GBSA (Prime molecular mechanics generalized-Born surface area) [8] is carried out. Surrounding amino acids within 12 Å of the inhibitor are treated flexibly (for MD relaxed complexes, only residues within 6 Å distance from the inhibitor are treated flexibly). The binding energy ($\Delta G_{\text{binding}}$) is evaluated as:

$$\Delta G_{\text{binding}} = \Delta E_{\text{MM}} + \Delta G_{\text{solvation}} + \Delta G_{\text{SA}}$$

where ΔE_{MM} is the difference between the minimized energies of the complex and the sum of the free inhibitor and receptor energies, $\Delta G_{\text{solvation}}$ is the GBSA solvation energies difference between the complex and the sum of the free inhibitor and receptor and ΔG_{SA} is the surface area energies difference between the complex and the sum of the free inhibitor and receptor.

QM/MM rescoring is performed on the MD relaxed complexes (M8 and M19) such that the inhibitor is treated at the QM level applying the B3LYP/LACVP* level of theory, while the rest of the system is treated at the MM level of theory applying the OPLS2005 force field and using Q-site [36,37]. Calculations are done using the QM/MM–PBSA script from Schrödinger and solvation effect is ignored.

For the binding energy evaluation from the trajectory, the MM/PBSA module of AMBER12 is used, trajectory snapshots are collected each 10 ps during the 1–10 ns simulation period, i.e. 900 snapshots are used [38].

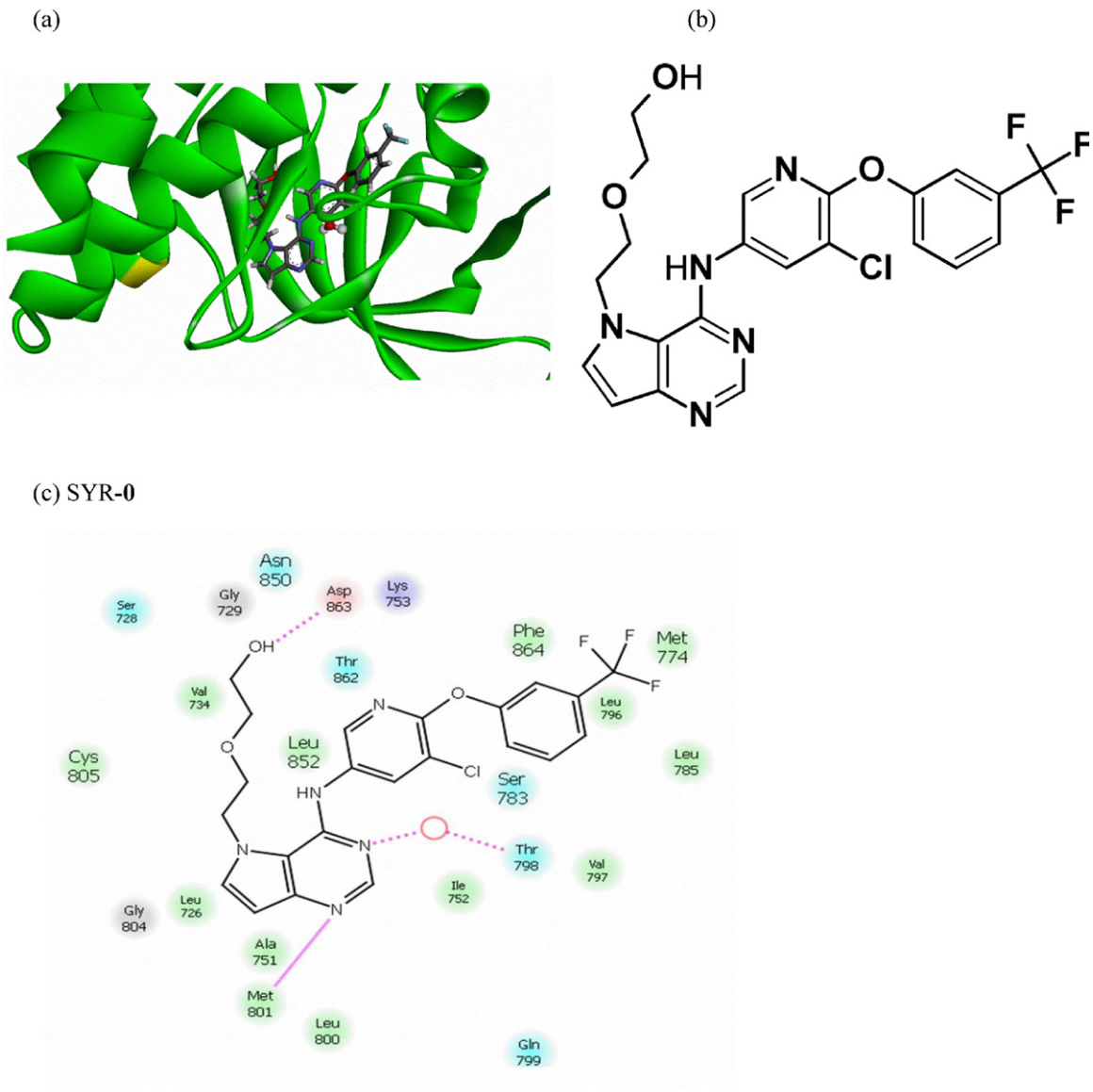

Fig. 1. (a) The crystal structure of the kinase domain of human epidermal growth factor receptor 2 co-crystallized with SYR; (b) 2D structure of SYR; (c) 2D inhibitor–protein interaction diagram showing the original pose of SYR (SYR-0).

3. Results and discussion

3.1. The IFD protocol

As can be seen in Fig. 1a, the inhibitor binding site in HER2 is located in a deep cleft connecting the N-terminal lobe (N-lobe) and the C-terminal lobe (C-lobe) called the hinge region, which is primarily the ATP binding site [13]. All inhibitors show a similar binding mode to the original inhibitor SYR (Fig. 3a). They are placed in the hinge region and form a strong H-bond with Met801. As shown in Fig. 3b and c (SYR-**I** and SYR-**II**), the IFD produced SYR poses agree quite well with the original pose (Fig. 3a, SYR-**0**). The maximum atomic RMSDs between the produced poses (Fig. 3, SYR-**I** and SYR-**II**) and the original pose (Fig. 3a, SYR-**0**) after superposition of all carbons are below 1.2 Å. For the IFD produced SYR poses, such as SYR-**I** and SYR-**II**, the pyrrolopyrimidine ring is placed in the receptor active site and is able to form strong H-bonds with the backbone amide of Met801. However, unlike the original SYR-**0**, these poses do not show the H-bond formed between the terminal hydroxyl group of the ethoxyethanol moiety and Asp863. Instead, they show H-bond interactions with other amino acids, for example Arg849 (SYR-**I**) or Asp808 (SYR-**II**). In addition only two poses out of the eleven IFD produced complexes correctly predict the N(3)···HOH H-bond.

In the present study, the new inhibitors are able to form several interactions with the receptor as shown in Fig. 4. The quinazoline ring nitrogens (ring **B**, Fig. 2) are able to form two H-bonds, one with the backbone N—H of Met801 (N1) and the other with the conserved water molecule.

Fig. 4 shows the two dimensional inhibitor–protein diagrams of the most active inhibitors, i.e. (a) M19-**I**, (b) M19-**II** and (c) M8-**I**. Utilizing visual inspection, The IFD generated poses for the new inhibitors can be divided into two main clusters. In the first one, inhibitor is superimposed on the original inhibitor (SYR-**0**), the hinge region accommodates the quinazoline ring, whereas the flexible part is accommodated by the deep hydrophobic pocket (selectivity pocket) formed of Leu796, Leu785, Met774, Ala771 and Phe864 (Fig. 4a, M19-**I**). In the second cluster, the two terminal rings of the inhibitors are flipped by approximately 100° (Fig. 4b, M19-**II**). This angle flipping implies some rearrangements of the residues in the vicinity, such as Phe731 and Lys753. Previous studies have shown that HER2 is more able (compared to EGFR) to accommodate

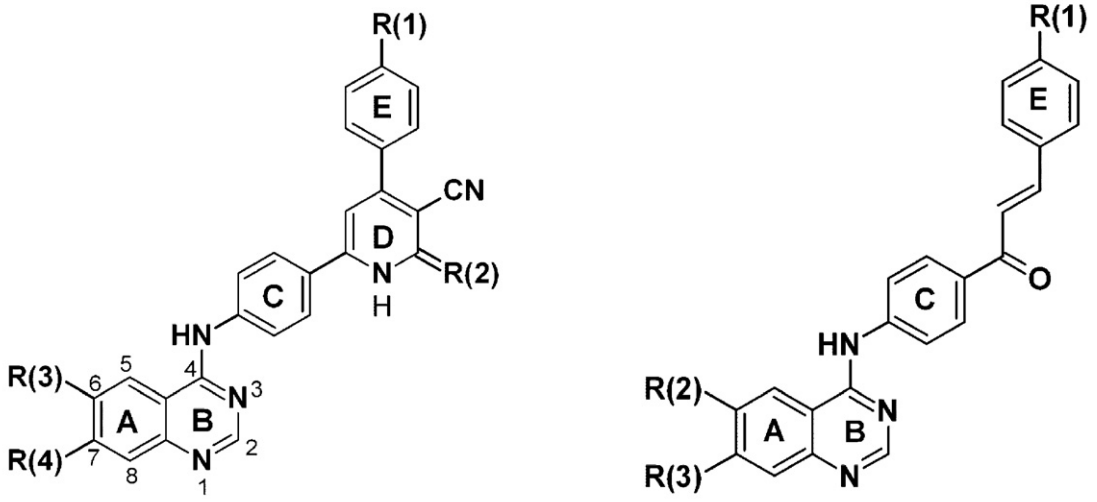

M1	R_1 = Cl	R_2 = O	R_3 = H	R_4 = H
M2	R_1 = OMe	R_2 = O	R_3 = H	R_4 = H
M3	R_1 = Br	R_2 = O	R_3 = H	R_4 = H
M4	R_1 = F	R_2 = O	R_3 = H	R_4 = H
M5	R_1 = Cl	R_2 = NH	R_3 = H	R_4 = H
M6	R_1 = OMe	R_2 = NH	R_3 = H	R_4 = H
M7	R_1 = Br	R_2 = NH	R_3 = H	R_4 = H
M8	R_1 = F	R_2 = NH	R_3 = H	R_4 = H
M17	R_1 = Cl	R_2 = O	R_3 = OMe	R_4 = OMe
M18	R_1 = OMe	R_2 = O	R_3 = OMe	R_4 = OMe
M19	R_1 = Br	R_2 = NH	R_3 = OMe	R_4 = OMe

M9	R_1 = Cl	R_2 = H	R_3 = H
M20	R_1 = Cl	R_2 = OMe	R_3 = OMe

Fig. 2. 2D structures of the inhibitors under study.

bulky substituents at the 4-anilino site of the 4-anilinoquinazoline inhibitors, that is selectivity to HER2 can be enhanced by increasing the size of the substituents on the 4-anilino site of the inhibitors [11,39], which is the case in the present study. For example, the measured IC_{50} of the most potent compound in vitro (M19) of the new series show lower values (i.e. higher potency) for HER2 versus EGFR inhibition (EGFR: 1.935 μM, HER2: 1.036 μM). This is in contrast to the measured IC_{50} value of M20, which shows enhanced activity toward EGFR (IC_{50} of 2.582 μM) than that for HER2 (IC_{50} of 99.96 μM). This is due to that the M20 inhibitor lacks the ring **D** (Fig. 2b), which decreases the bulkiness of the 4-anilino group and reduces the ability of the inhibitor to fully occupy the selectivity pocket.

As discussed before, the measured IC_{50} of M19 against HER2 is determined to be 1.035 μM, which makes it the most potent inhibitor in this series in vitro, it is able to form several H-bonds according to the poses generated by the IFD protocol. Inhibitor M19-**I** (see Fig. 4a) forms strong H-bonds with Met801 (1.959 Å), the water molecule (2.014 Å) and Gln799 (2.258 Å). Two extra H-bonds (salt bridges) are formed by the internal N-H of ring (**D**) with Asp863 (which is similar to SYR-**0**) and the other H-bond is formed by the external imino group of the same ring with Lys753 positively charged terminal ammonium group ($-NH_3^+$). The terminal ring (**E**) penetrates deeply in the pocket (Fig. 4a and b), which seems to rearrange to accommodate the bulky 4-anilino moiety. Similarly, the obtained poses of M8 (IC_{50} of 3.981 μM) suggest it to be a strong binder to HER2 through H-bonds network of Met801, Gln799 and Lys753 (see Fig. 4c).

Other inhibitors in the series exhibit a similar binding mode as does for M19 and M8, and various substituents (Fig. 2a and b) give raise to different activity profiles. For inhibitors (M1–M4), where R_2 = O, R_3 = R_4 = H and R_1 is the substitution site, it is clear that higher activities are achieved if R_1 is substituted by an electron donating group, such as a methoxy group rather than a halogen atom. Also, for the halogen, the lower the electronegativity the higher the activity such that higher activity is achieved if R_1 = Br rather than Cl or F atoms. Almost all poses of this group of inhibitors (M1–M4) are of the second cluster of poses in which the terminal rings (**D** and **E**) are flipped by approximately 100° from the corresponding original poses (see Fig. 5a). The next group of inhibitors (M5–M8) where R_2 = NH, R_3 = R_4 = H and R_1 is the substitution site, show poses belonging to both clusters with higher proportion for those poses belonging to the first cluster (see Fig. 5b). This is because of the H-bond formation between the —NH group of ring **D** and the Asp863 backbone carbonyl and/or the one formed between external imino group of the same ring with Lys753 positively charged terminal ammonium group (see above). The first group of inhibitors (M1–M4) lacks this —NH group so that this H-bonding interaction is missing. Other inhibitors such as M17 and M18 show poses from both clusters.

For the rest of inhibitors in Fig. 2, i.e. M17–M20, the dimethoxy tail at ring **A** (R_3 and R_4) seems to play an important role in the inhibitory activity of this class of inhibitors. Substitution at these two positions by two methoxy groups in M7 which inhibits the enzymatic activity of HER2 by 2% gives M19 which has an 85% inhibition. Other inhibitors show similar trend to a lesser extent. For example M1 and M17 (19–43%), M9 and M20 (2–18%), also attributing to the replacement with the dimethoxy tails at R_3 and R_4.

Tables 1 and 2 represent the binding energy scores of the inhibitors in the present study. Those in Table 1 are for the IFD produced complexes. Table 2 presents the binding energy scores for complexes for which MD simulations are carried out. As shown in Table 1, inhibitors binding energies scores exhibit a poor correlation with the experimental %inhibition. This may be due to different starting protein conformations of the IFD complexes, as noticed earlier by Delgado-Soler et al. [5]. For example, the Prime-MM/GBSA binding energy scores of nearly half of the inhibitors are

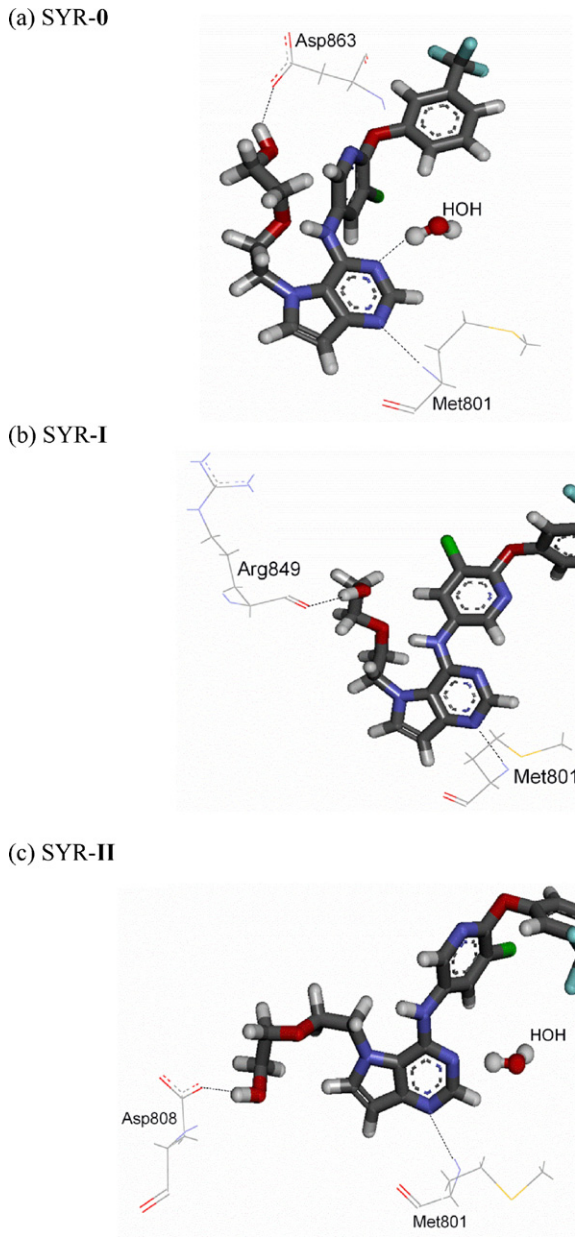

Fig. 3. Comparison between the original pose of SYR (SYR-**0**) (a), and two different IFD generated poses of SYR (b) SYR-**I** and (c) SYR-**II**.

more than 100 kcal/mol that is M1, M3, M6, M9 and M18 whereas the %inhibition ranges from 2% to 35% for the same set of inhibitors. The IFD score, however, show a slightly better Pearson correlation coefficient (r) with experimental %inhibition of about 0.42.

3.2. Molecular dynamic simulation

In the present study, complexes formed between the protein and the two most potent inhibitors, i.e. M19 and M8 are studied using a 10 ns MD simulation in the NVT ensemble to fully account for the flexibility of the inhibitor–protein interactions. Fig. 6a represents the root mean square deviation (RMSD) calculations of the protein backbone Cα atoms using ptraj. The simulation is stable with a maximum RMSD of about 2.5 Å and the two trajectories start to diverge after 1 ns and converge again after 6 ns until the end of the simulation time. (For temperature and energy conservation, see Supporting info.)

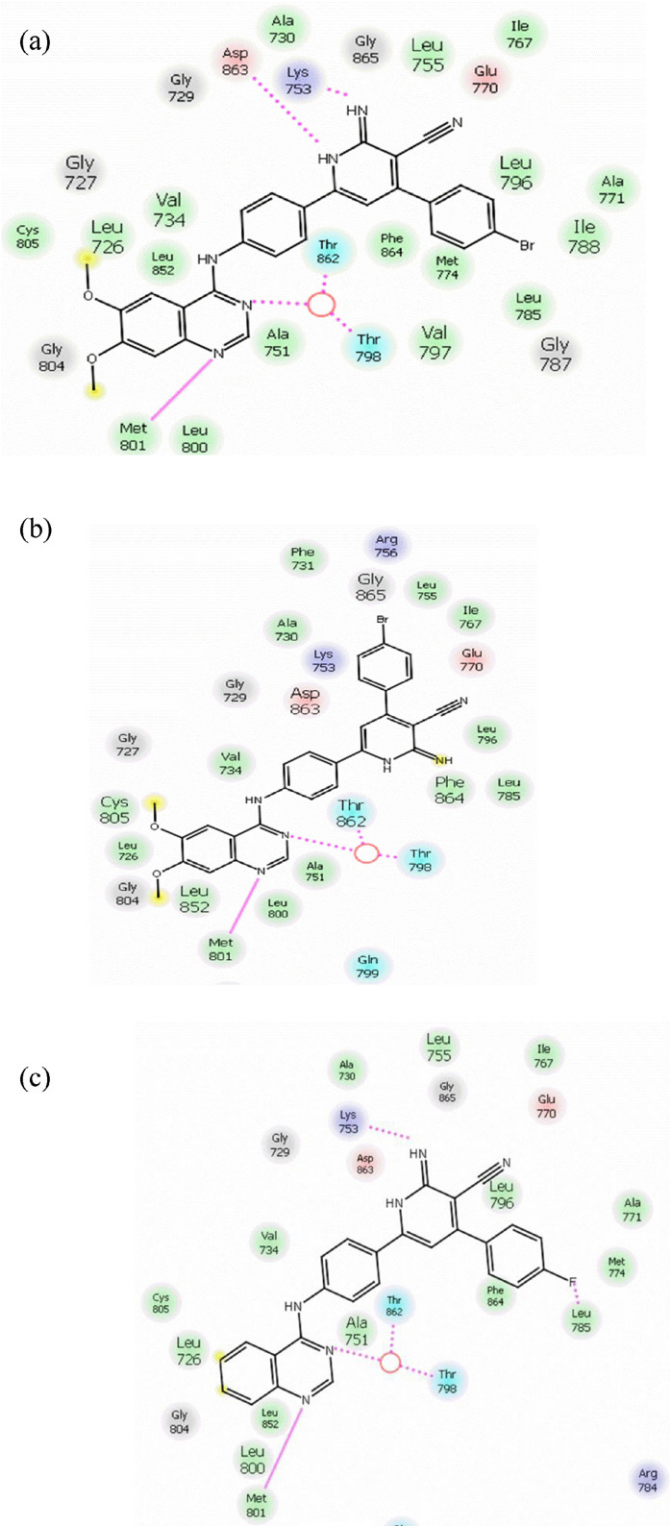

Fig. 4. 2D inhibitor–protein interaction diagram of (a) M19-**I**; (b) M19-**II**; and (c) M8-**I**.

The distances of two H-bonds have been monitored during the entire 10 ns simulation of the two complexes using the H-bond tool in VMD [40]. One is the most important inhibitor-N(1)···H-Met801 bond in the hinge region of the HER2 receptor (see Fig. 6b). The average distance is about 2 Å, indicating that this H-bond is indeed all the time strong. Both inhibitors M8 and M19 tend to show some larger fluctuation but they are quiet stable in the

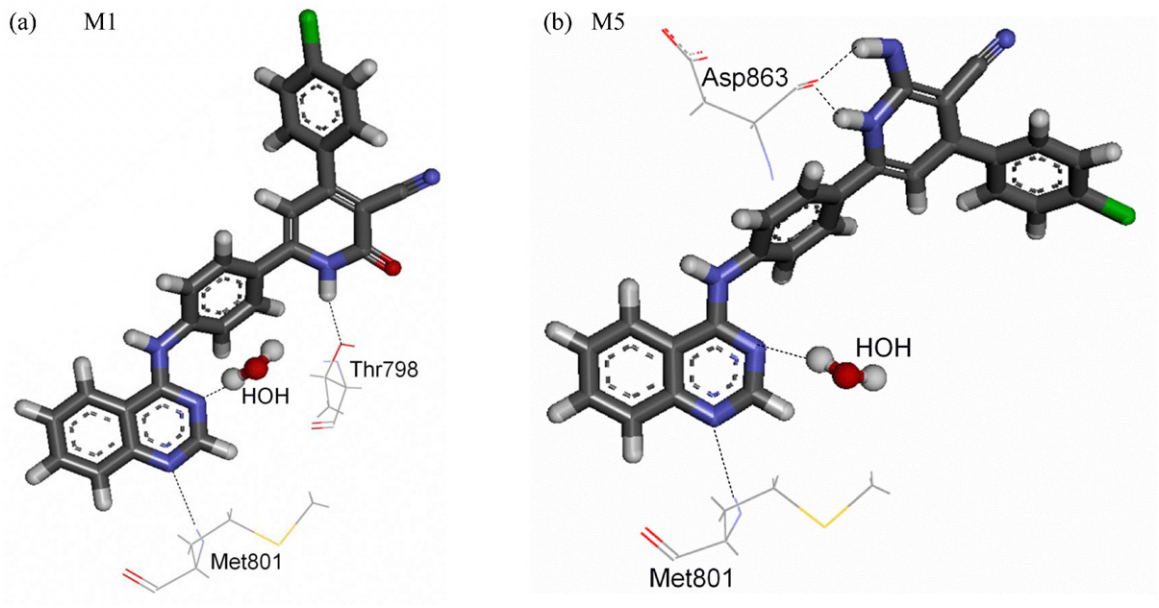

Fig. 5. The docking pose of (a) M1 and (b) M5 in the active site of HER2 produced by the IFD protocol.

Table 1
Experimental %inhibition together with simulated binding energies and scores for the IFD produced complexes (kcal/mol).

Title	XP G-score	IFD score	Prime-MM/GBSA DG bind[a]	%Inhibition (5 μM)
M1	−14.38	−645.09	−100.48	19
M2	−14.43	−646.65	−87.17	40
M3	−15.13	−645.59	−113.00	35
M4	−15.02	−644.71	−93.15	19
M5	−15.09	−644.39	−72.24	15
M6	−13.35	−643.58	−106.12	25
M7	−15.58	−644.30	−80.90	2
M9	−12.54	−642.11	−116.21	2
M17	−13.17	−645.20	−85.69	43
M18	−14.91	−648.49	−118.98	18
M20	−13.27	−646.19	−93.62	18

[a] Residues within 12 Å of the inhibitor are treated flexibly.

rest of the simulation. The second hinge region H-bond is the inhibitor-H(2)···O-Gln799. This H-bond is considered to be important measure to monitor packing in the hinge region by different inhibitors which possess an extra tail in the quinazoline ring, such as the one present in erlotinib or M19 in the present case [16]. As exhibited in Fig. 6c, this H-bond has larger distances with the average of 2.7 Å, the maximum fluctuation for M19 occurs after about 0.4 ns to reach a maximum of 3.9 Å. Similarly, for M8 the same maximum is reached after 5.2 ns. This can be attributed to the presence of the dimethoxy tails that push the inhibitor for better filling and packing of the hinge region.

Table 3
Total and decomposed binding energies of the MD studied complexes (kcal/mol).

Contribution	Title	
	M8	M19
ΔE_{ele}	−17.35	−17.57
ΔE_{vdW}	−55.49	−65.05
$\Delta G_{binding}$ (AMBER-PBSA)[a]	−72.03	−82.18
$\Delta G_{binding}$ (AMBER-GBSA)[a]	−43.49	−53.13

[a] $\Delta G_{binding} = \Delta E_{ele} + \Delta E_{vdW} + \Delta G_{solvation}$.

Apart from the hinge regions, other amino acid residues also play roles in the binding process, such as Asp863 and Lys753.

3.3. MM/GBSA and MM/PBSA

Table 2 represents the different scoring and binding energy calculations of the two MD produced complexes applying different terms and scoring methods. Both the QM/MM and the MM based methods show consistency with the experimental inhibitory profiles of both inhibitors measured in vitro. Individual binding energy components, i.e. electrostatic and vdW (ΔE_{ele} and ΔE_{vdW}) obtained through a trajectory analysis using the MMPBSA script of AMBER are supplied in Table 3. As expected, the major term that favors the binding in this class of receptors is the vdW term. M19 seems to have higher contribution from both terms (ΔE_{ele} and ΔE_{vdW}) than M8 although higher effects comes from the vdW term, which is given by −65.05 kcal/mol for M19 and −55.49 kcal/mol for M8.

Table 2
Experimental %inhibition together with simulated binding energies and scores for the MD produced complexes (kcal/mol).

Title	$\Delta E_{QM/MM}$[a]	Prime-MM/GBSA DG bind[b]	XP G-score	IFD-score	IC_{50} (μM)	%Inhibition[c]
M19	−59.99	−116.73	−13.25	−644.65	1.035	85
M8	−32.09	−87.02	−12.18	−640.02	3.981	54
SYR	−105.44	−124.30	–	–	0.011[d]	–

[a] Calculations are carried out using the QM/MM–PBSA script from Schrödinger and ignoring solvation, the B3LYP/LACVP*//OPLS2005 level of theory is applied, QM substructure composed of inhibitor atoms only.
[b] Residues within 6 Å of the inhibitor are treated flexibly.
[c] At 5 μM concentration.
[d] See Ref. [13]. Binding energy calculations are performed on the prepared crystal structure.

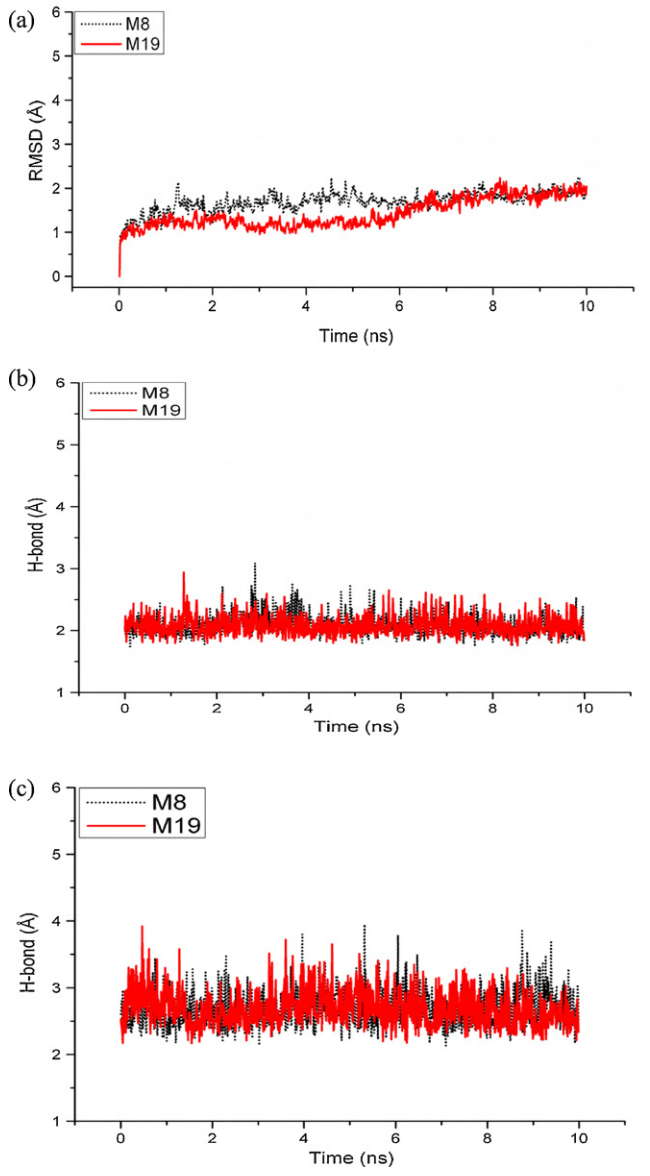

Fig. 6. (a) Root mean square deviation (RMSD) plots of the backbone α-carbons, solvent exposed N-terminal residues (706–720) are not considered, (b) H-bond distances of N(1) of the two bound inhibitors and the Met801 backbone nitrogen and (c) H-bond distances of C(2)-H of the two bound inhibitors and the Gln799 backbone carbonyl oxygen during the 10 ns molecular dynamics simulation runs.

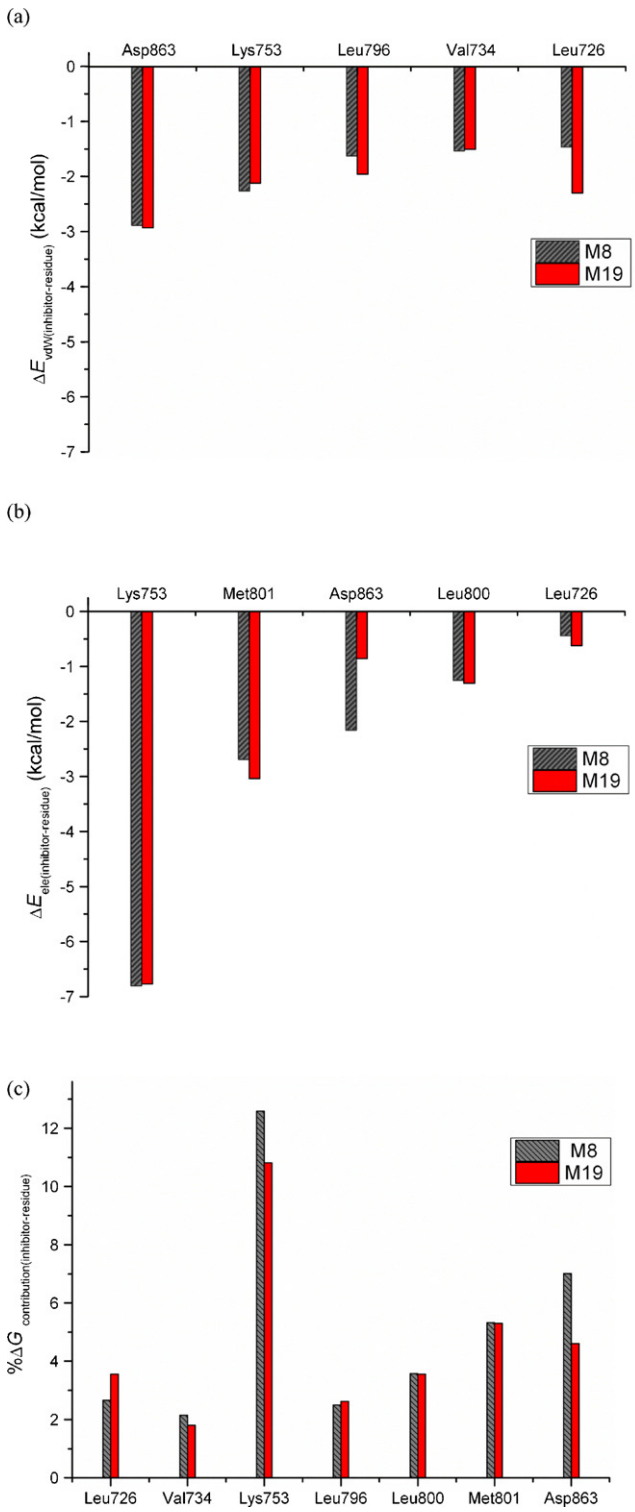

Fig. 7. Per-residue binding energy decomposition of the two inhibitor–protein complexes during the 1–10 ns MD simulation, (a) per-residue contribution to the vdW interaction and (b) per-residue contribution to the electrostatic interaction; (c) total residue contribution to the total binding energy.

For further better understanding of individual components that favor the binding, energy of binding is further decomposed on a per-residue interaction basis using the MMPBSA method. Fig. 7a and b displays a two bar plots for the individual binding energy components (ΔE_{ele} and ΔE_{vdW}) on a per-residue interaction basis for the favorable residues. For the ΔE_{vdW}, although both molecules do not show a great difference, a higher contribution from the Leu726 residue as a result of the presence of the dimthoxy tail in M19 only. The highest contribution to the ΔE_{vdW} comes from the Asp863 residue, which also contribute to the ΔE_{ele} term although to a lesser extent. For the ΔE_{ele} term, the highest contribution comes from the Lys753 residue, which forms a salt bridge – see above – with the external imino group of ring **D**. The second most important residue in this term is the Met801, which makes a stable anchoring point (H-bond) to the N(1) of the bound inhibitor. The contribution is slightly higher in case of M19 (−3.04 kcal/mol) than M8 (−2.7 kcal/mol). Fig. 7c also represents the per-residue %contribution to the total binding energy. As shown in the figure, highest contribution comes primarily from the two extra-hinge (with respect to the quinazoline core) residues Lys753 and Asp863. Knowing that in most cases resistance to current chemotherapeutic agents comes primarily because of mutation in the nearby residues of the quinazoline core, the new series may provide an insight toward designing inhibitors

that are more able to overcome the problem of resistance. Research in this direction is currently in progress.

4. Conclusion

In order to assess the potency of a series of a recently synthesized anilioquinazoline HER2 inhibitors, a combined docking, scoring and molecular dynamic simulations have been carried out. The IFD is successful in reproducing the binding pose of the original inhibitor. The results of the MD simulation show that the new synthesized inhibitors are stable in the binding site of the HER2 receptor and is able to form various interactions with the receptor in the hinge region, as well as two observed stable charge assisted H-bonds (salt bridges) with Asp863 and Lys753. Decomposition of the binding energy shows that vdW interaction is the most important factor to derive binding and that certain amino acid residues are particularly important.

Acknowledgements

MA acknowledges the Swinburne University Postgraduate Research Award (SUPRA). National Computational Infrastructure (NCI) at the Australian National University for the award under the Merit Allocation Scheme, Victorian Partnership for Advanced Computing (VPAC) and Swinburne University Supercomputing Facilities Green/Gstar machines are acknowledged. MA also acknowledges Jeff Saunders from Schrödinger inc. for his help and assistance.

Appendix A. Supplementary data

Supplementary data associated with this article can be found, in the online version, at http://dx.doi.org/10.1016/j.jmgm.2012.12.001.

References

[1] D.B. Kokh, R.C. Wade, W. Wenzel, Receptor flexibility in small-molecule docking calculations, WIREs Computational Molecular Science 1 (2011) 298–314.
[2] B. Waszkowycz, D.E. Clark, E. Gancia, Outstanding challenges in protein–ligand docking and structure-based virtual screening, WIREs Computational Molecular Science 1 (2011) 229–259.
[3] A.C. Anderson, R.H. O'Neil, T.S. Surti, R.M. Stroud, Approaches to solving the rigid receptor problem by identifying a minimal set of flexible residues during ligand docking, Chemistry and Biology 8 (2001) 445–457.
[4] W. Sherman, H.S. Beard, R. Farid, Use of an induced fit receptor structure in virtual screening, Chemical Biology & Drug Design 67 (2006) 83–84.
[5] L. Delgado-Soler, J. Ariñez-Soriano, J. Granadino-Roldán, J. Rubio-Martinez, Predicting binding energies of CDK6 inhibitors in the hit-to-lead process, Theoretical Chemistry Accounts: Theory, Computation, and Modeling/Theoretica Chimica Acta 128 (2011) 807–823.
[6] H. Alonso, A.A. Bliznyuk, J.E. Gready, Combining docking and molecular dynamic simulations in drug design, Medicinal Research Reviews 26 (2006) 531–568.
[7] H. Zhong, L.M. Tran, J.L. Stang, Induced-fit docking studies of the active and inactive states of protein tyrosine kinases, Journal of Molecular Graphics and Modelling 28 (2009) 336–346.
[8] J. Du, H. Sun, L. Xi, J. Li, Y. Yang, H. Liu, X. Yao, Molecular modeling study of checkpoint kinase 1 inhibitors by multiple docking strategies and prime/MM–GBSA calculation, Journal of Computational Chemistry 32 (2011) 2800–2809.
[9] M.M. Gottesman, T. Fojo, S.E. Bates, Multidrug resistance in cancer: role of ATP-dependent transporters, Nature Reviews Cancer 2 (2002) 48–58.
[10] G. Szakacs, J.K. Paterson, J.A. Ludwig, C. Booth-Genthe, M.M. Gottesman, Targeting multidrug resistance in cancer, Nature Reviews Drug Discovery 5 (2006) 219–234.
[11] M. Arkin, M. Moasser, HER-2-directed small-molecule antagonists, Current Opinion in Investigational Drugs 9 (2008) 1264–1276.
[12] M.M. Sadek, R.A. Serrya, A.N. Kafafy, M. Ahmed, F. Wang, K.A. Abouzid, Discovery of new HER2/EGFR dual kinase inhibitors based on anilinoquinazoline scaffold as potential anti-cancer agents, submitted for publication.
[13] K. Aertgeerts, R. Skene, J. Yano, B.-C. Sang, H. Zou, G. Snell, A. Jennings, K. Iwamoto, N. Habuka, A. Hirokawa, T. Ishikawa, T. Tanaka, H. Miki, Y. Ohta, S. Sogabe, Structural analysis of the mechanism of inhibition and allosteric activation of the kinase domain of HER2 protein, Journal of Biological Chemistry 286 (2011) 18756–18765.
[14] W. Sherman, T. Day, M.P. Jacobson, R.A. Friesner, R. Farid, Novel procedure for modeling ligand/receptor induced fit effects, Journal of Medicinal Chemistry 49 (2005) 534–553.
[15] Schrödinger Suite, Protein Preparation Wizard; Epik version 2.2, Schrödinger, LLC, New York, 2011; Impact version 5.7, Schrödinger, LLC, New York, 2011; Prime version 3.0, Schrödinger, LLC, New York, 2011.
[16] V. Aparna, G. Rambabu, S.K. Panigrahi, J.A.R.P. Sarma, G.R. Desiraju, Virtual screening of 4-anilinoquinazoline analogues as EGFR kinase inhibitors: importance of hydrogen bonds in the evaluation of poses and scoring functions, Journal of Chemical Information and Modeling 45 (2005) 725–738.
[17] B. Zhang, V.B.C. Tan, K.M. Lim, T.E. Tay, Significance of water molecules in the inhibition of cylin-dependent kinase 2 and 5 complexes, Journal of Chemical Information and Modeling 47 (2007) 1877–1885.
[18] E. Muzzioli, A. Del Rio, G. Rastelli, Assessing protein kinase selectivity with molecular dynamics and MM–PBSA binding free energy calculations, Chemical Biology & Drug Design 78 (2011) 252–259.
[19] T.E. Balius, R.C. Rizzo, Quantitative prediction of fold resistance for inhibitors of EGFR, Biochemistry 48 (2009) 8435–8448.
[20] M.P. Jacobson, D.L. Pincus, C.S. Rapp, T.J.F. Day, B. Honig, D.E. Shaw, R.A. Friesner, A hierarchical approach to all-atom protein loop prediction, Proteins: Structure, Function, and Bioinformatics 55 (2004) 351–367.
[21] Prime, version 3.0, Schrödinger, LLC, New York, 2011.
[22] M.J. Frisch, et al., Gaussian09, Rev A.02, Gaussian Inc., Wallingford, CT, 2009.
[23] Schrödinger Suite. Induced Fit Docking Protocol, 2011; Glide version 5.7, Schrödinger, LLC, New York, NY, 2011; Prime version 3.0, Schrödinger, LLC, New York, NY, 2011.
[24] Glide, version 5.7, Schrödinger, LLC, New York, 2011.
[25] R.A. Friesner, R.B. Murphy, M.P. Repasky, L.L. Frye, J.R. Greenwood, T.A. Halgren, P.C. Sanschagrin, D.T. Mainz, Extra precision glide: docking and scoring incorporating a model of hydrophobic enclosure for protein–ligand complexes, Journal of Medicinal Chemistry 49 (2006) 6177–6196.
[26] D.A. Case, et al., AMBER 12, University of California, San Francisco, 2012.
[27] Y. Duan, C. Wu, S. Chowdhury, M.C. Lee, G. Xiong, W. Zhang, R. Yang, P. Cieplak, R. Luo, T. Lee, J. Caldwell, J. Wang, P. Kollman, A point-charge force field for molecular mechanics simulations of proteins based on condensed-phase quantum mechanical calculations, Journal of Computational Chemistry 24 (2003) 1999–2012.
[28] V. Hornak, R. Abel, A. Okur, B. Strockbine, A. Roitberg, C. Simmerling, Comparison of multiple Amber force fields and development of improved protein backbone parameters, Proteins: Structure, Function, and Bioinformatics 65 (2006) 712–725.
[29] B. Mennucci, J. Tomasi, R. Cammi, J.R. Cheeseman, M.J. Frisch, F.J. Devlin, S. Gabriel, P.J. Stephens, Polarizable continuum model (PCM) calculations of solvent effects on optical rotations of chiral molecules, Journal of Physical Chemistry A 106 (2002) 6102–6113.
[30] C.I. Bayly, P. Cieplak, W. Cornell, P.A. Kollman, A well-behaved electrostatic potential based method using charge restraints for deriving atomic charges: the RESP model, Journal of Physical Chemistry 97 (1993) 10269–10280.
[31] J. Wang, R.M. Wolf, J.W. Caldwell, P.A. Kollman, D.A. Case, Development and testing of a general amber force field, Journal of Computational Chemistry 25 (2004) 1157–1174.
[32] W.L. Jorgensen, J. Chandrasekhar, J.D. Madura, R.W. Impey, M.L. Klein, Comparison of simple potential functions for simulating liquid water, Journal of Chemical Physics 79 (1983) 926–935.
[33] J.-P. Ryckaert, G. Ciccotti, H.J.C. Berendsen, Numerical integration of the cartesian equations of motion of a system with constraints: molecular dynamics of n-alkanes, Journal of Computational Physics 23 (1977) 327–341.
[34] H.J.C. Berendsen, J.P.M. Postma, W.F. van Gunsteren, A. DiNola, J.R. Haak, Molecular dynamics with coupling to an external bath, Journal of Chemical Physics 81 (1984) 3684–3690.
[35] T. Darden, D. York, L. Pedersen, Particle mesh Ewald: An $N\cdot\log(N)$ method for Ewald sums in large systems, Journal of Chemical Physics 98 (1993) 10089–10092.
[36] R.B. Murphy, D.M. Philipp, R.A. Friesner, A mixed quantum mechanics/molecular mechanics (QM/MM) method for large-scale modeling of chemistry in protein environments, Journal of Computational Chemistry 21 (2000) 1442–1457.
[37] QSite, version 5.7, Schrödinger, LLC, New York, 2011.
[38] T. Hou, J. Wang, Y. Li, W. Wang, Assessing the performance of the MM/PBSA and MM/GBSA methods. 1. The accuracy of binding free energy calculations based on molecular dynamics simulations, Journal of Chemical Information and Modeling 51 (2010) 69–82.
[39] D.W. Fry, Mechanism of action of erbB tyrosine kinase inhibitors, Experimental Cell Research 284 (2003) 131–139.
[40] W. Humphrey, A. Dalke, K. Schulten, VMD: visual molecular dynamics, Journal of Molecular Graphics 14 (1996) 33–38.